Ctr2 regulates biogenesis of a cleaved form of mammalian Ctr1 metal transporter lacking the copper- and cisplatin-binding ecto-domain

Helena Öhrvik[a,1], Yasuhiro Nose[a,1], L. Kent Wood[a,1,2], Byung-Eun Kim[a,3], Sophie-Charlotte Gleber[b], Martina Ralle[c], and Dennis J. Thiele[a,4]

[a]Department of Pharmacology and Cancer Biology, Duke University School of Medicine, Durham, NC 27708; [b]X-Ray Science Division, Advanced Photon Source, Argonne National Laboratory, Argonne, IL 60439; and [c]Department of Biochemistry and Molecular Biology, Oregon Health and Science University, Portland, OR 97239

Edited by Michael A. Marletta, The Scripps Research Institute, La Jolla, CA, and approved October 1, 2013 (received for review June 21, 2013)

Copper is an essential catalytic cofactor for enzymatic activities that drive a range of metabolic biochemistry including mitochondrial electron transport, iron mobilization, and peptide hormone maturation. Copper dysregulation is associated with fatal infantile disease, liver, and cardiac dysfunction, neuropathy, and anemia. Here we report that mammals regulate systemic copper acquisition and intracellular mobilization via cleavage of the copper-binding ecto-domain of the copper transporter 1 (Ctr1). Although full-length Ctr1 is critical to drive efficient copper import across the plasma membrane, cleavage of the ecto-domain is required for Ctr1 to mobilize endosomal copper stores. The biogenesis of the truncated form of Ctr1 requires the structurally related, previously enigmatic copper transporter 2 (Ctr2). Ctr2$^{-/-}$ mice are defective in accumulation of truncated Ctr1 and exhibit increased tissue copper levels, and X-ray fluorescence microscopy demonstrates that copper accumulates as intracellular foci. These studies identify a key regulatory mechanism for mammalian copper transport through Ctr2-dependent accumulation of a Ctr1 variant lacking the copper- and cisplatin-binding ecto-domain.

uptake | platinum | protein regulation | endosome | lysosome

Due to its unique chemistry, the redox-active metal ion copper (Cu) is an essential element for human growth and development (1–3). Defects in Cu metabolism are associated with pathologies that include Alzheimer's disease, peripheral neuropathy, anemia, neutropenia, cardiomyopathy, Menkes disease, and Wilson's disease (4–9). Although many of the components responsible for Cu uptake, intracellular distribution, detoxification, and efflux have been identified, the mechanisms by which these proteins are regulated are not well understood.

The copper transporter 1 (Ctr1) protein is a high-affinity Cu^+ transporter that functions in copper accumulation in organisms ranging from yeast to mammals (10–16). In mammals Ctr1 localizes to both the plasma membrane and to intracellular vesicles (17–19). Mice bearing a systemic Ctr1 deletion fail to survive gestation, whereas tissue-specific ablation of Ctr1 in the intestinal epithelium, liver, or heart cause a range of phenotypes that include peripheral Cu deficiency, hepatic iron accumulation, and lethal cardiac hypertrophy, respectively (20–24). Moreover, both yeast and mammalian Ctr1 function in acquisition of the chemotherapeutic agent cisplatin (25–29) and Ctr1 expression levels have been correlated to the efficacy of chemotherapy and patient survival (30). The regulation of Ctr1 function and abundance is of great significance to both normal growth and development as well as to the efficacy of platinum-based chemotherapy.

The general structure and function of Ctr1 is conserved from yeast to humans, with three membrane-spanning domains and a Met-X_3-Met motif in the second transmembrane domain that is essential for Cu^+ import (16). The human and mouse protein contains a short ecto-domain with clusters of Met and His. Mutagenic and truncation studies in the context of intact yeast or human Ctr1 indicate that the ecto-domain in general, and the Met residues in particular, play an important role in high-affinity cellular Cu^+ import, yet all but one key Met near the first transmembrane domain appear to be dispensable for function in cellular Cu^+ import (31). Studies using model peptides suggest that the Ctr1 Met residues are direct ligands for both Cu^+ and cisplatin (32–34). In contrast to Cu^+ uptake, the Met-rich ecto-domain of yeast Ctr1 is required for cisplatin import (27). Moreover, as Ctr1 M-X_3-M mutants are competent for cisplatin uptake, but not Cu^+ (35), studies suggest that Ctr1-mediated cisplatin uptake may occur via an ecto-domain–dependent receptor-mediated endocytosis mechanism, rather than as an ion channel as for Cu^+ (27). Ctr1 has been observed in both cell lines and mouse tissues as a full-length glycosylated form and a lower-molecular-weight form, which has been reported to lack a portion of the Cu^+ and cisplatin-binding ecto-domain (17, 36). However, neither the physiological significance of this truncated form of Ctr1, nor its mode of biogenesis, have been elucidated.

The Ctr2 protein is structurally related to Ctr1 and is encoded by a linked gene in both the mouse and the human genome. Recent studies suggest that Ctr2 functions as a low-affinity Cu^+ importer, a lysosomal Cu^+ exporter, or as a regulator of cellular

Significance

Copper is essential for normal growth and development because it serves roles in catalysis, signaling, and structure. Cells acquire copper through the copper transporter 1 (Ctr1) protein, a copper transporter that localizes to the cell membrane and intracellular vesicles. Both copper and the anticancer drug cisplatin are imported by Ctr1 by virtue of an extracellular domain rich in metal-binding amino acids. In this report we demonstrate that a protein structurally related to Ctr1, called Ctr2, plays a role in the generation or stability of a truncated form of Ctr1 lacking a large portion of the extracellular domain. Retention of this domain in mice or cells lacking Ctr2 enhances copper and cisplatin uptake, thereby establishing Ctr2 as a regulator of Ctr1 function.

Author contributions: H.Ö., Y.N., L.K.W., B.-E.K., M.R., and D.J.T. designed research; H.Ö., Y.N., L.K.W., B.-E.K., S.-C.G., and M.R. performed research; S.-C.G. and M.R. acquired and analyzed XFM images; H.Ö., Y.N., L.K.W., B.-E.K., M.R., and D.J.T. analyzed data; and H.Ö., Y.N., and D.J.T. wrote the paper.

The authors declare no conflict of interest.

This article is a PNAS Direct Submission.

[1]H.Ö., Y.N., and L.K.W. contributed equally to this article.

[2]Present address: DuPont Pioneer Hi-Bred International, Johnston, IA 50131.

[3]Present address: Department of Animal and Avian Sciences, University of Maryland, College Park, MD 20742.

[4]To whom correspondence should be addressed. E-mail: dennis.thiele@duke.edu.

This article contains supporting information online at www.pnas.org/lookup/suppl/doi:10.1073/pnas.1311749110/-/DCSupplemental.

macropinocytosis (37–39). However, these studies have been performed in cultured cells, and the physiological role of Ctr2 in animals has not been reported. Here we demonstrate that Ctr2 interacts with Ctr1 in vivo and that Ctr2 knockout mice show increased levels of total copper in several tissues. Mice and mouse embryonic fibroblasts lacking Ctr2 accumulate copper in endosomal compartments and have lower levels of the truncated form of Ctr1 lacking the metal-binding ecto-domain. Whereas truncation of the Ctr1 ecto-domain reduces Cu^+ import at the plasma membrane, truncated Ctr1 stimulates the mobilization of Cu^+ from endosomal compartments. These studies demonstrate a critical role for Ctr2 in modulating the accumulation of Ctr1 lacking the Cu^+ and cisplatin-binding ecto-domain of Ctr1 and, as a consequence, in the regulation of cellular copper uptake and intracellular mobilization. Given the fundamental role for Ctr1 in Cu^+ import and cisplatin acquisition, the action of Ctr2 represents an important mechanism for the regulation of Ctr1 function.

Results

Ctr2 Knockout Mice Accumulate Cu. The protein encoded by the mammalian Ctr2 gene shares many features in common with the Ctr1 high-affinity Cu^+ importer, including three predicted transmembrane domains and an M-X_3-M motif in the second transmembrane domain that is essential for Cu^+ import by Ctr1 in organisms from yeast to mammals (Fig. 1*A*). Ctr2 lacks the Met-rich and His-rich clusters found in the ecto-domain of Ctr1 that have been shown to bind Cu^+ and contribute to high-affinity Cu^+ uptake and also lacks the His-Cys-His motif found within the Ctr1 cytosolic tail. Furthermore, the Ctr1 and Ctr2 chromosomal loci are tightly linked (~73 kb) with the *Fkbp15* gene intervening (Fig. S1*A*).

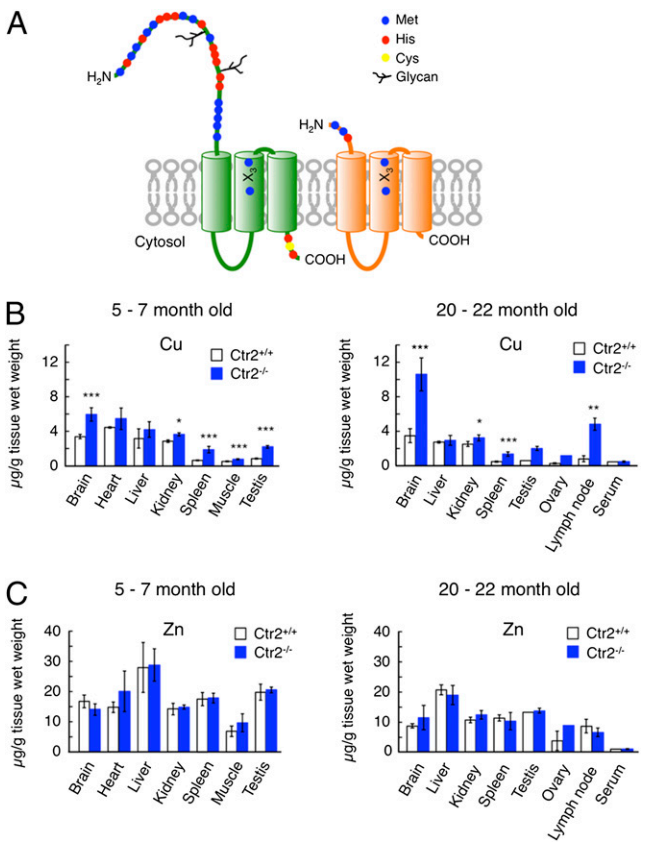

Fig. 1. Loss of Ctr2 results in increased copper levels in tissue. (*A*) Topological models for Ctr1 and Ctr2 showing transmembrane domains and a conserved M-X_3-M motif. The Ctr1 ecto-domain has two glycosylation sites and clusters of Met and His residues, with two Met and one His in the Ctr2 ecto-domain. (*B*) Wild-type and $Ctr2^{-/-}$ age-matched mice 5–7 and 20–22 mo were analyzed for tissue copper levels by ICP-MS. (*C*) Zn analysis as in *B*. Data presented as mean ± SD from two to eight mice. See Fig. S1 for generation of Ctr2 knockout mice.

To investigate the physiological function of Ctr2, a systemic knockout of the *Ctr2* gene was generated in mice (Fig. S1 *B–D*). In general, the $Ctr2^{-/-}$ mice grow normally, with no obvious developmental defects. Surprisingly, copper levels in tissues are significantly elevated in brain, kidney, spleen, muscle, and testes in 5- to 7-mo-old $Ctr2^{-/-}$ mice and was exacerbated in brain tissue from 20- to 22-mo-old mice (Fig. 1*B*). No significant differences were observed between wild-type and $Ctr2^{-/-}$ mice for copper in the liver or for the accumulation of Zn (Fig. 1*C*) or Fe in any tissue. The Ctr2 gene excision on mouse chromosome 4 did not affect expression of the linked Fkbp15 protein (Fig. S1*E*). These data demonstrate that Ctr2 plays a specific role in copper accumulation in a physiological context and that mice lacking Ctr2 accumulate copper to levels significantly above that of wild-type animals.

The expression of Ctr1 and Ctr2 mRNA in several mouse tissues was evaluated by RNA blotting. As shown in Fig. S1*F*, the Ctr2 probe detects two mRNA species of ~1.3 and 2.4 kb, with the larger species more abundant in all tissues evaluated with the exception of mouse testes. As previously observed, two mRNA species are detected for Ctr1 of ~1.6 and 4.5 kb, with highest expression in liver, kidney, and testes (15). Interestingly, the steady-state levels of mRNAs encoding Ctr1 and Ctr2 were highest in heart, liver, kidney, and testes, suggesting the possibility that the encoded proteins may act in the same biological process.

Ctr1 is an integral membrane protein that localizes both to the plasma membrane and to intracellular vesicles that constitutively cycle to and from the plasma membrane (40). Previous reports suggested that Ctr2 protein localizes to intracellular vesicles and, to a lesser extent, the plasma membrane (37, 39). Because Ctr2 encodes a predicted integral membrane protein, experiments were conducted to investigate its membrane topology. Ctr2 was expressed with either an amino-terminal FLAG epitope (FLAG-Ctr2) or a carboxyl-terminal FLAG epitope (Ctr2-FLAG). Although FLAG-Ctr2 protein was detected in nonpermeabilized cells, Ctr2-FLAG could be detected only in permeabilized cells (Fig. S1*G*). These results suggest that ectopically expressed Ctr2 harbors a membrane topology that is similar to that shown for Ctr1, with a cytoplasmic carboxyl-terminus.

Copper Accumulates in Intracellular Deposits in $Ctr2^{-/-}$ Mouse Brain. Mice lacking Ctr2 exhibit no overt defects in growth or development, although many tissues accumulate copper, with brain copper being particularly high (Fig. 1*B*). To further characterize the nature of the copper that accumulates in $Ctr2^{-/-}$ mice, X-ray fluorescence microscopy (XFM) (41) was carried out on saggitally sectioned brains from 5-mo-old wild-type and $Ctr2^{-/-}$ littermates. Scans of the cortex and caudoputamen revealed dramatic differences in copper accumulation between wild-type and $Ctr2^{-/-}$ brain (Fig. 2 *A* and *B*). Although the copper distribution was consistently even (and concentrations were low) in scans for wild-type brain, all scanned areas of the $Ctr2^{-/-}$ brain revealed tightly localized copper deposits throughout. These deposits were between 1.5 and 3 μm in diameter and exhibited copper concentrations that were on average ~40-fold higher than surrounding areas. The magnified overlay of the two-dimensional elemental maps for phosphorous (P, indicative of nuclei) and copper (Cu) suggests that these copper deposits are localized outside of the nucleus (Fig. 2 *A* and *B*).

Whereas the area copper concentrations in wild-type brain ranged from ~40 to 70 μM (2.5–4.4 μg/g tissue), those for $Ctr2^{-/-}$ were between 60 μM to 149 μM (3.7–9.2 μg/g tissue) (Table S1).

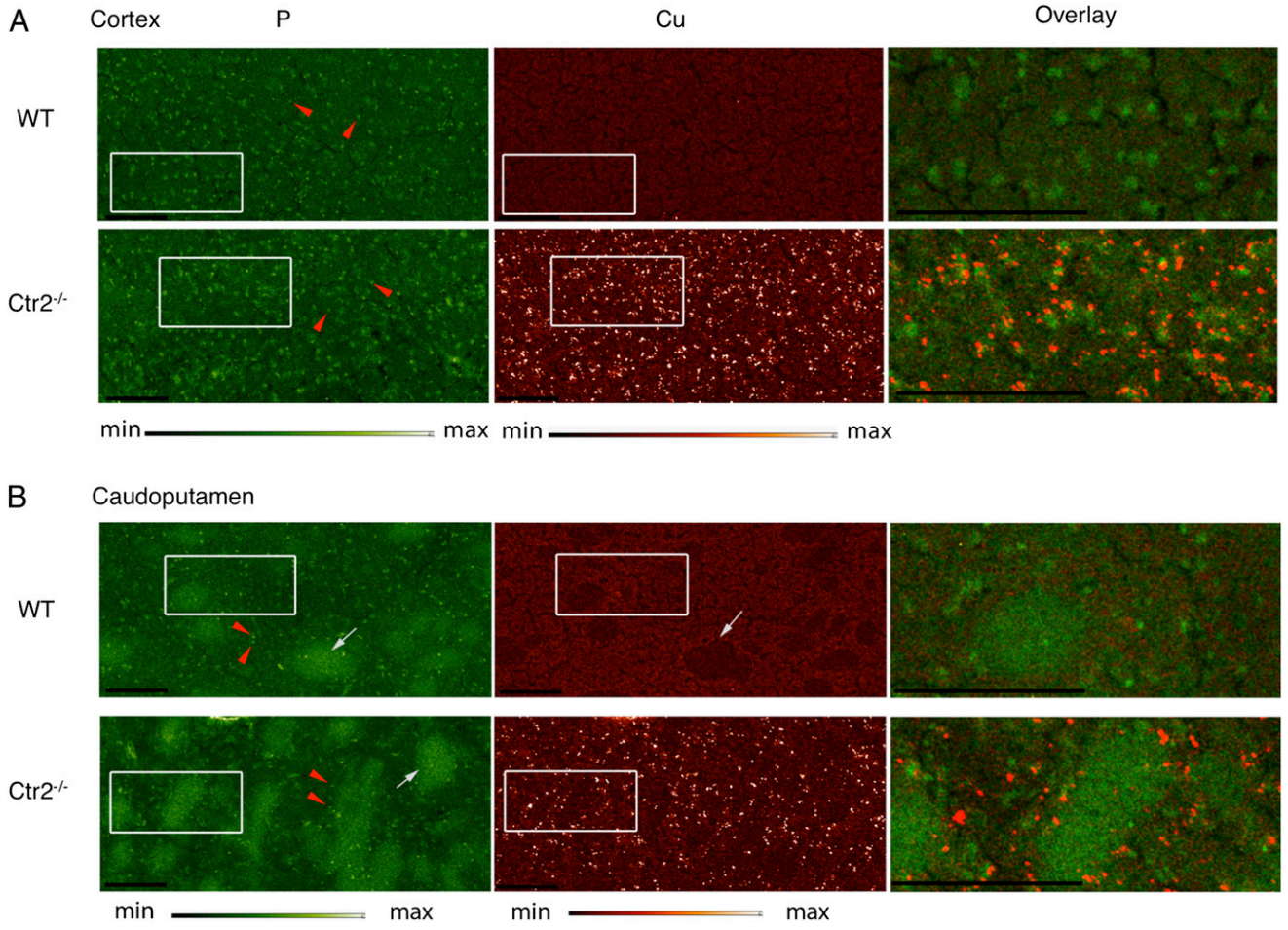

Fig. 2. Copper accumulates in intracellular deposits in Ctr2$^{-/-}$ mouse brain. (*A*) XFM images for phosphorous (P, green) and copper (Cu, red) and a magnified overlay from the cortex for a Ctr2$^{+/+}$ (*Upper*) and a Ctr2$^{-/-}$ (*Lower*) mouse. (Scale bar, 50 μm.) The false coloring scheme for P and Cu is shown below images. The intensity of the fluorescence signal is displayed as a linear scale (P:0 – ≥11 μg/cm^2; Cu:0 – ≥0.03 μg/cm^2). In the P map, nuclei are visible (red arrows). The overlay for the magnified area shows an intracellular localization for the copper foci. (*B*) XFM image of the caudoputamen for littermate Ctr2$^{+/+}$ (*Upper*) and Ctr2$^{-/-}$ (*Lower*) mice exhibiting two-dimensional elemental maps for phosphorous (P, green), copper (Cu, red), and a magnified overlay. Nuclei are visible in the P-map. Pencil fibers in the caudoputamen (white arrows). (See Table S1 for Cu and P concentrations in other brain regions determined by XFM.)

The XFM-derived copper concentrations are in good agreement with bulk inductively coupled plasma mass spectrometry (ICP-MS) measurements of digests from the complementary brain halves and for whole brains (Fig. 1*B* and Table S1). Taken together, XFM studies demonstrate that Ctr2$^{-/-}$ mice strikingly accumulate copper in brain tissue, where it is localized to intracellular deposits.

Ctr2$^{-/-}$ Mouse Embryonic Fibroblasts Show Increased Total Copper Levels and Intracellular Cu Deposits. To gain mechanistic insights into why copper levels increase in Ctr2$^{-/-}$ mice and localize to intracellular foci, immortalized mouse embryonic fibroblasts (MEFs) were generated from wild-type and Ctr2$^{-/-}$ littermates (Fig. S2 *A* and *B*). Metal analysis demonstrated that Ctr2$^{-/-}$ MEFs accumulated copper, but not Zn, compared with wild-type MEFs (Fig. 3*A*). Moreover, whereas transfection of Ctr2$^{-/-}$ MEFs with an empty expression vector did not alter copper levels, expression of the Ctr2 cDNA resulted in cellular copper levels similar to that of wild-type MEFs, with no significant alteration in Zn accumulation (Fig. 3*B*).

XFM analysis of Ctr2$^{-/-}$ mouse brain demonstrated strong accumulation of copper in intracellular foci. To investigate whether these copper deposits occur only in the context of the whole animal, or in a cell-autonomous manner, both wild-type and Ctr2$^{-/-}$ MEFs were stained with the live-cell Cu$^+$-specific fluorescent sensor, CS3. As shown with a representative field in Fig. 3*C*, wild-type MEFs exhibited fluorescence in a largely pan-cellular fashion, with small punctate spots. Ctr2$^{-/-}$ MEFs also showed a pan-cellular fluorescence pattern, but with intense large punctate staining, not unlike the intracellular copper deposits detected in Ctr2$^{-/-}$ mouse brain by XFM. These observations suggest that the appearance of copper foci is a cell-autonomous phenomenon due to the loss of Ctr2.

Copper Accumulates in an Endosomal Compartment in Ctr2$^{-/-}$ MEFs. Both Ctr2$^{-/-}$ mouse brain and Ctr2$^{-/-}$ MEFs accumulate copper at higher levels relative to wild type, and imaging studies suggest that this copper accumulates as intracellular foci. To explore the nature of these foci, both wild-type and Ctr2$^{-/-}$MEFs were subjected to subcellular fractionation to resolve endosomal compartments (Fig. S3), and fractions were analyzed for copper content (Fig. 4*A*). The results show a fivefold increase in copper levels in fraction 1 from Ctr2$^{-/-}$ MEFs compared with the same fraction from wild-type MEFs. The copper concentrations in fraction 2 did not differ between the Ctr2$^{+/+}$ and Ctr2$^{-/-}$ cells, and copper levels in fraction 3 were below the detection limit for both cell lines. Protein extracts from the fractions were immunoblotted for Ctr2, Ctr1, and for markers of the endosomal, ly-

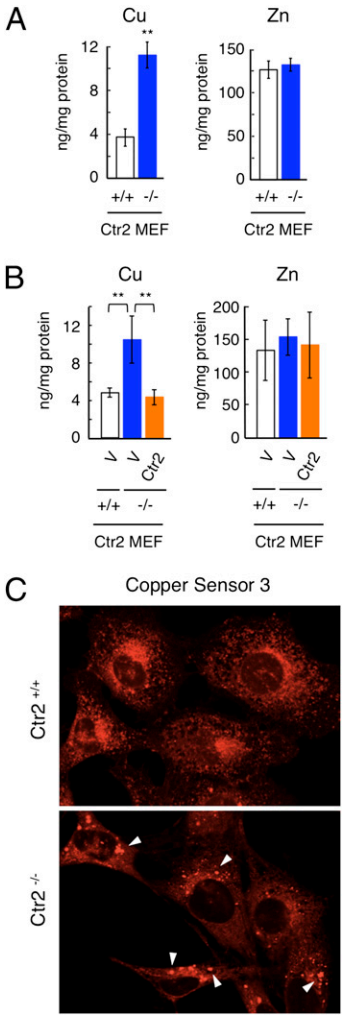

Fig. 3. Ctr2$^{-/-}$ MEFs accumulate copper in punctae. (*A*) Wild-type and Ctr2$^{-/-}$ MEFs were analyzed for total copper and Zn levels by ICP-MS. (*B*) Expression of the Ctr2 cDNA (Ctr2) but not the empty vector (V) re-establishes low copper levels without changes in Zn levels. Data are presented as mean ± SD from four biological replicates. (*C*) Wild type (Ctr2$^{+/+}$) and Ctr2$^{-/-}$ MEFs were stained with the membrane-permeable Cu^{+}-specific stain CS3 and photographed by confocal microscopy. White arrowheads point to large punctate staining. (See Fig. S2 for PCR design of Ctr2 genotyping in the Ctr2 MEFs and genotyping of the Ctr2 MEFs.)

sosomal, cytosolic, and mitochondrial-enriched compartments (Fig. 4*B*). Ctr2 localized to fraction 1 in the Ctr2$^{+/+}$ cells. This same fraction, which harbors the accumulated copper from Ctr2$^{-/-}$ MEFs, also has the bulk of Ctr1, which extended into fractions 2 and 3 for the Ctr2$^{-/-}$ MEFs in some fractionation experiments. Fraction 1 also contains the lysosomal marker Lamp1, the early endosomal markers Rab4 and Rab5, the late endosomal markers Rab7 and Rab9, and the recycling endosome marker Rab11. However, Rab9- and Rab11-positive vesicles are enriched in fraction 1, suggesting that Ctr2 preferentially cosediments with late endosomes directed toward the transgolgi network (TGN) and recycling endosomes to or from the plasma membrane. It is notable that fraction 1 was enriched for lysosomes and endosomes, but also shows some contamination with the plasma membrane as revealed by the detection of Na/K–ATPase. The mitochondrial marker CoxIV was detected only in fractions 2 and 3, with no apparent overlap with Ctr2. Together, these subcellular fractionation data demonstrate that Ctr1 and Ctr2 are abundant in endosomes recycling from and to the plasma membrane, as well as in late endosomes trafficking to the TGN. In addition, when Ctr2 is absent, copper accumulates in these late endosomes.

Both Ctr1 and Ctr2 have been reported to form homo-multimers (31, 37, 42). Given the results presented here, demonstrating that Ctr2 loss increases intracellular copper levels and that Ctr1 and Ctr2 cosediment in endosomes, we ascertained whether Ctr1 and Ctr2 associate in vivo. c-Myc epitope-tagged Ctr2 (Myc-Ctr2) and FLAG epitope-tagged Ctr1 ($FLAG_2$-Ctr1) were expressed in HEK293T cells either alone or in combination, in cells treated with the membrane-permeable cross-linker dithiobis[succinimidyl propionate] (DSP); Ctr1 was immunoprecipitated with anti-FLAG antibody and immunoblotted with anti–c-Myc antibody. As shown in Fig. 4*C*, immunoprecipitation of $FLAG_2$-Ctr1 by the anti-FLAG beads coprecipitated Myc-Ctr2 only when both proteins were coexpressed. Immunoprecipitation of Myc-Ctr2 also coprecipitated $FLAG_2$-Ctr1, but was

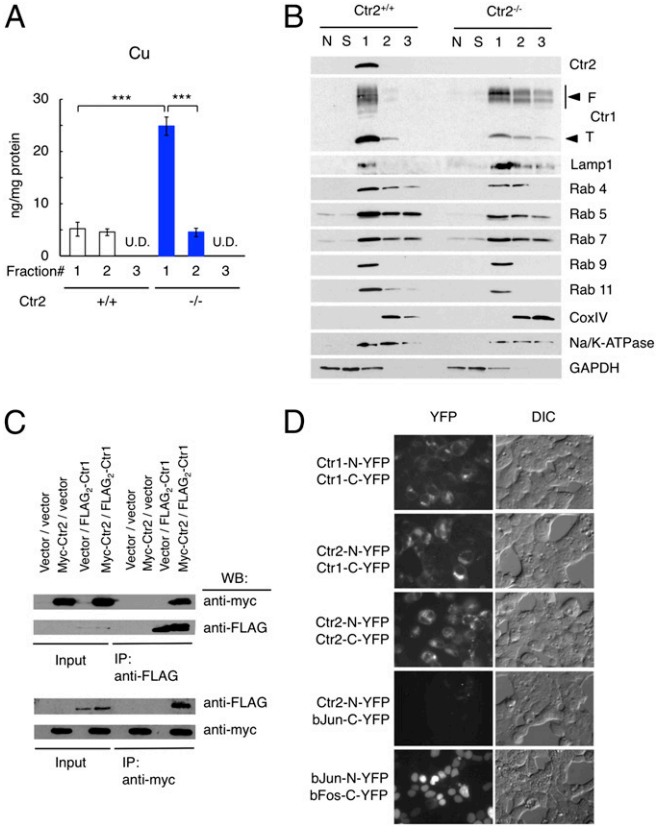

Fig. 4. Copper accumulates in endosomes in Ctr2$^{-/-}$ MEFs. (*A*) Copper was measured (ng/mg protein) in each of three subcellular fractions from wild-type (Ctr2$^{+/+}$) and Ctr2$^{-/-}$ MEFs (see Fig. S3*A* for fractions collected from the iodixanol gradient). Shown are the results (mean ± SD) from six biological replicates for each fractionation. (*B*) Immunoblotting of protein extracts derived from subcellular fractionation experiments outlined in Fig. S3*A* from wild-type and Ctr2$^{-/-}$ MEFs. Blots were analyzed by probing with anti-Ctr2, anti-Ctr1 (T, truncated; F, full-length), anti-Lamp1, anti-Rab4, anti-Rab5, anti-Rab7, anti-Rab9, anti-Rab11, anti-CoxIV, anti-Na/K-ATPase, and anti-GAPDH. (*C*) Ctr1 and Ctr2 reciprocally coimmunoprecipitate from solubilized protein extracts. HEK293T cells were transfected with the indicated expression vector or empty vector and treated with DSP crosslinker; proteins were immunoprecipitated with the indicated antibody (IP), and proteins were analyzed by immunoblotting with the indicated antibody (WB). (See Fig. S3*B* for co-IP without cross-linker) (*D*) Ctr1 and Ctr2 associate in BiFC assays. HEK293T cells were transfected with the indicated pairs of expression plasmids and photographed by fluorescence microscopy and differential interference contrast microscopy (DIC).

not observed in cells with empty vector or expressing only one of the proteins. Similar results were also observed in the absence of cross-linker, albeit at lower levels of detection (Fig. S3*B*).

To independently evaluate the potential for interactions between Ctr1 and Ctr2 in live cells, a bimolecular fluorescence complementation (BiFC) assay was used (43). Plasmids expressing fusion proteins between Ctr1 and amino- or carboxyl-terminal fragments of YFP (Ctr1-*N*-YFP, Ctr1-C-YFP) and Ctr2 and YFP fragments (Ctr2-*N*-YFP, Ctr2-C-YFP) and other plasmids were transfected into HEK293T cells. Expression of any one protein fused to the carboxyl- or amino-terminal fragment of YFP did not give rise to a detectable fluorescent signal. As shown in Fig. 4*D*, cotransfection with Ctr1-C-YFP and Ctr1-*N*-YFP resulted in a positive signal, indicative of protein–protein interactions for this well-established homo-trimeric molecule. Consistent with a previous report that Ctr2 multimerizes in cultured cells (37), coexpression of Ctr2-*N*-YFP and Ctr2-C-YFP gave a positive signal in the BiFC assay. Moreover, coexpression of Ctr2-*N*-YFP with Ctr1-C-YFP gave a positive fluorescence signal, indicating that Ctr1 and Ctr2 are present in a complex in vivo. Although coexpression of Fos-*N*-YFP with bJun-C-YFP was positive for this well-characterized heterodimeric bZip domain transcription factor complex, Ctr2-*N*-YFP and Fos-C-YFP did not give rise to a positive signal, indicating specificity for the observed positive interactions. Together, these data indicate that Ctr1 and Ctr2 can form a direct or indirect protein complex in mammalian cells.

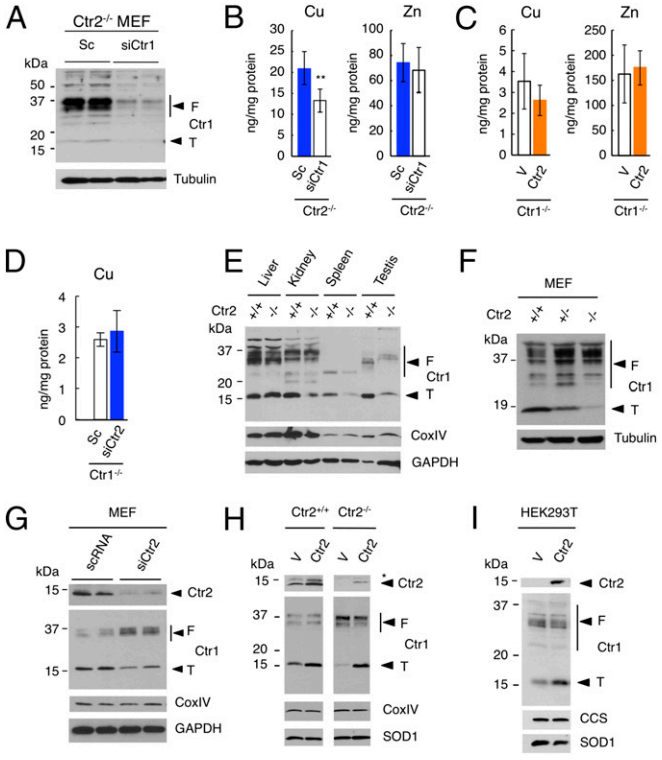

Fig. 5. Ctr2$^{-/-}$ MEFs show Ctr1-dependent copper accumulation. (*A*) Silencing of Ctr1 (siCtr1) in two independent experiments, but not scrambled RNA (Sc), results in depletion of Ctr1 protein levels. Full-length Ctr1 (F) and truncated Ctr1 (T) are shown with tubulin as a loading control. (*B*) Silencing of Ctr1 reduces Cu accumulation in Ctr2$^{-/-}$ MEFs with no change in Zn levels. (*C*) Overexpression of Ctr2 in Ctr1$^{-/-}$ MEFs does not alter copper or Zn levels. (*D*) Silencing of Ctr2 in Ctr1$^{-/-}$ MEFs does not alter copper levels. Data presented as mean ± SD from four biological replicates. (*E*) Protein extracts from the indicated tissues from wild-type mice and Ctr2$^{-/-}$ littermates were immunoblotted with anti-Ctr1, anti-CoxIV, and anti-GAPDH antibody. Shown are the full-length (F) and truncated (T) forms of Ctr1. (*F*) Protein extracts from wild-type, Ctr2$^{+/-}$, and Ctr2$^{-/-}$ MEFs were analyzed as in *A* but with anti-tubulin antibody as loading control. (*G*) Silencing of Ctr2 (siCtr2) in wild-type MEFs resulted in a decrease in the levels of truncated Ctr1 compared with scRNA. Extracts were analyzed as in *E*. (*H*) Overexpression of Ctr2-enhanced Ctr1 ecto-domain cleavage in wild-type cells and restored Ctr1 cleavage in Ctr2$^{-/-}$ cells. Cells were transfected with empty vector (V) or the vector with Ctr2 cDNA (Ctr2) and protein extracts were analyzed as in *E* with SOD1 detected as loading control. (*I*) Expression of mouse Ctr2 enhances human Ctr1 ecto-domain cleavage. HEK293T cells were transfected with an empty vector (V) or a vector with the Ctr2 cDNA (Ctr2), and protein extracts were analyzed with anti-Ctr1, anti-CCS, and anti-SOD1 antibody. (See Fig. S5 for ATP7A protein expression in wild-type and Ctr2$^{-/-}$ mice and MEFs, and localization of ATP7A in the Ctr2 MEFs.)

Ctr2$^{-/-}$ MEFs Exhibit Ctr1-Dependent Copper Accumulation and Reduced Ctr1 Truncation. To date, Ctr1 is the only high-affinity Cu^+ importer identified in mammals. To ascertain the contribution of Ctr1 to the accumulation of copper in Ctr2$^{-/-}$ MEFs, siRNA was used to dampen the expression of Ctr1 in Ctr2$^{-/-}$ MEFs, and copper accumulation was measured. As shown in Fig. 5*A*, an siRNA against Ctr1 resulted in a strong, although incomplete, reduction in steady-state Ctr1 protein levels in two independent experiments compared with a scrambled RNA. Furthermore, knockdown of Ctr1 in Ctr2$^{-/-}$ MEFs partially alleviated the accumulation of copper, whereas no changes in Zn levels were observed (Fig. 5*B*). Overexpression of Ctr2 in the Ctr1$^{-/-}$ MEFs did not affect the steady-state levels of copper or Zn (Fig. 5*C*). Moreover, RNAi of Ctr2 in Ctr1$^{-/-}$ MEFs resulted in no change in intracellular copper levels (Fig. 5*D*). These results suggest that Ctr2 is not a copper importer and that the accumulation of copper observed in Ctr2$^{-/-}$ MEFs is at least partially dependent on Ctr1. Consistent with this observation, expression of mammalian Ctr1 in yeast lacking high-affinity Cu^+ transporters rescued the copper-dependent growth phenotype, but expression of Ctr2 was unable to do so (Fig. S4).

Although data presented here demonstrate the participation of Ctr1 in copper accumulation in Ctr2$^{-/-}$ MEFs, it is possible that Ctr2 also functions to negatively regulate the expression, trafficking, or activity of ATP7A or ATP7B, two Cu^+-exporting ATPase pumps whose inactivation results in copper accumulation in cells or tissues (6). Because ATP7B has a dominant role in hepatic copper excretion and liver copper levels were not significantly elevated in Ctr2$^{-/-}$ mice (Fig. 1*B*), we ascertained whether ATP7A expression is altered in Ctr2$^{-/-}$ mice and Ctr2$^{-/-}$ MEFs compared with their wild-type counterparts. As shown in Fig. S5*A*, levels of ATP7A do not change in Ctr2$^{-/-}$ mice compared with wild-type animals. Furthermore, neither ATP7A protein levels in Ctr2$^{-/-}$ mouse tissues or Ctr2$^{-/-}$ MEFs nor the basal or copper-induced trafficking of ATP7A from the TGN to the plasma membrane were altered in Ctr2$^{-/-}$ MEFs compared with wild-type cells (Fig. S5 *A*–*C*).

The observations that reduction of Ctr1 levels by RNAi ameliorated the copper accumulation in Ctr2$^{-/-}$ MEFs and knockdown of Ctr2 did not affect the copper levels in Ctr1$^{-/-}$ MEFs suggest that Ctr2 functions in copper import, at least in part, via the regulation of Ctr1 expression or activity. The abundance of Ctr1 in several tissues from wild-type and Ctr2$^{-/-}$ littermates was analyzed by immunoblotting with a polyclonal antibody directed against the Ctr1 intracellular loop domain. In mouse tissues and in cultured cells, Ctr1 appears as a glycosylated full-length form and a form that is truncated within the amino-terminal ecto-domain. Hepatic levels of the full-length and truncated forms of Ctr1 did not differ in the Ctr2$^{-/-}$ mouse in comparison with the wild type (Fig. 5*E*). However, the levels of truncated Ctr1 were significantly reduced in kidney and more so in spleen and testis in the Ctr2$^{-/-}$ mice compared with wild-type littermates, suggesting a correlation between copper accumulation (Fig. 1*B*) and reduced levels of truncated Ctr1. The levels of CoxIV, a mitochondrial cytochrome oxidase subunit

whose levels directly correlate with copper levels (44), were unchanged (Fig. 5*E*). Evaluation of Ctr1 by immunoblotting of extracts from wild-type, $Ctr2^{+/-}$, and $Ctr2^{-/-}$ MEFs demonstrated a direct correlation between Ctr2 gene dosage and the abundance of truncated Ctr1 (Fig. 5*F*).

We tested, by using RNAi, whether differences in the abundance of truncated Ctr1 in $Ctr2^{-/-}$ mice and MEFs might be due to unanticipated genomic alterations around the Ctr2 gene. As shown in Fig. 5*G*, treatment of wild-type MEFs with RNAi against Ctr2, but not scrambled RNAi, resulted in a reduction in Ctr2 protein levels and a corresponding reduction in truncated Ctr1 and increased full-length Ctr1. Furthermore, overexpression of the Ctr2 cDNA in wild-type MEFs resulted in increased truncated Ctr1, and expression of the Ctr2 cDNA, but not empty vector in $Ctr2^{-/-}$ MEFs, increased the abundance of truncated Ctr1 (Fig. 5*H*). CoxIV levels were unaltered in these experiments (Fig. 5 *G* and *H*). Moreover, expression of mouse Ctr2 in human HEK293T cells also resulted in elevated levels of truncated human Ctr1, without changes in CCS, the copper chaperone for SOD1 whose levels are reduced via proteasomal degradation when copper levels are elevated (Fig. 5*I*) (45). These results demonstrate that Ctr2 levels are important for the generation or stability of truncated Ctr1 and that abundance of truncated Ctr1 inversely correlates with copper accumulation in mice and cultured cells. Given the observations that neither ATP7A trafficking nor CCS or CoxIV protein levels are altered, the accumulated copper in $Ctr2^{-/-}$ mouse tissues and MEFs is not sensed in the cytosolic or mitochondrial compartments.

Truncated Ctr1 Facilitates Endosomal Copper Mobilization. A truncated form of human Ctr1 has been shown to have significantly reduced Cu^{+} import activity (36). Although neither the physiological role of truncated Ctr1 nor the nature of the cleavage site(s) have been characterized, previous studies speculated that human Ctr1 cleavage may occur within a five-amino-acid region 29–34 amino acids from the amino-terminus (46). We directly characterized the cleavage site of mouse Ctr1 by purifying the cleaved form and determining its sequence by mass spectrometry. A mouse Ctr1 protein with a carboxyl-terminal FLAG epitope tag (Ctr1-$FLAG_2$) was expressed in human HEK293T cells and truncated Ctr1 was gel-purified (Fig. S5). In-gel trypsin digestion followed by tandem liquid chromatography-mass spectroscopy (LC-MS) from two independent experiments revealed predominant cleavage sites within the Ctr1 ecto-domain after Met residues at positions 47, 48, and 51 (Fig. 6*A*). Notably, cleavage of mouse Ctr1 at these positions results in the removal of all 11 His residues and 10–13 Met residues in the Ctr1 ecto-domain, many of which have been shown to serve as Cu and cisplatin ligands in model peptides (32, 33, 47). Interestingly, Mets 49 and 51, which remain in the truncated Ctr1 protein, are essential for human Ctr1 function in Cu^{+} transport (31). Although both mouse and human Ctr1 proteins harbor Met- and His-rich ecto-domains, and both have been observed as full-length and truncated forms, their sequences are not identical within the ecto-domain. We carried out similar sequencing experiments in duplicate using a carboxyl-terminal FLAG epitope-tagged human Ctr1. As shown in Fig. 6*A*, human Ctr1 was cleaved in human cells predominantly within the run of Met residues in the ecto-domain at positions 40, 41, 42, and 45.

A previous report suggested that Ctr2 functions as a lysosomal copper exporter because overexpressed Ctr2 partially localized to the lysosome and modestly induced transcription from a metal-responsive reporter plasmid (37). Data presented here demonstrate that Ctr2 is important for the accumulation of truncated Ctr1, regulates Ctr1-mediated Cu^{+} accumulation, and prevents copper accumulation in the endosomal compartment. Given that Ctr1 localizes to both the plasma membrane and the endosomal compartment, we tested the possibility that truncated Ctr1, rather than Ctr2 or full-length Ctr1, mobilizes copper from endosomes. $Ctr2^{-/-}$ MEFs were transfected with an empty vector or plasmids that express Ctr2, wild-type Ctr1, or a truncated version of mouse Ctr1 in which translation begins at position 49. Expression of Ctr2 restored the generation of high levels of truncated Ctr1 (Fig. 6*B*). Expression of full-length Ctr1 resulted in the generation of both full-length and truncated Ctr1, whereas expression of truncated Ctr1 gave strongly elevated levels of the truncated form of the protein. Parallel cell samples were stained with CS3 to image Cu^{+} pools in live cells, and CS3-positive large punctae were quantified. $Ctr2^{-/-}$ cells accumulate intense copper punctae that, based on fractionation results, are likely to correspond to the endosomal compartment. Expression of wild-type Ctr2 in $Ctr2^{-/-}$ MEFs resulted in a reduction in CS3-positive large punctae by ~50%, and a modest reduction was also observed by expressing wild-type Ctr1 (Fig. 6 *C* and *D*). Expression of truncated Ctr1, in the absence of Ctr2, reduced the number of large CS3-positive punctae to approximately the same level as that observed by expressing Ctr2. Furthermore, as shown in Fig. 6*E*, truncated

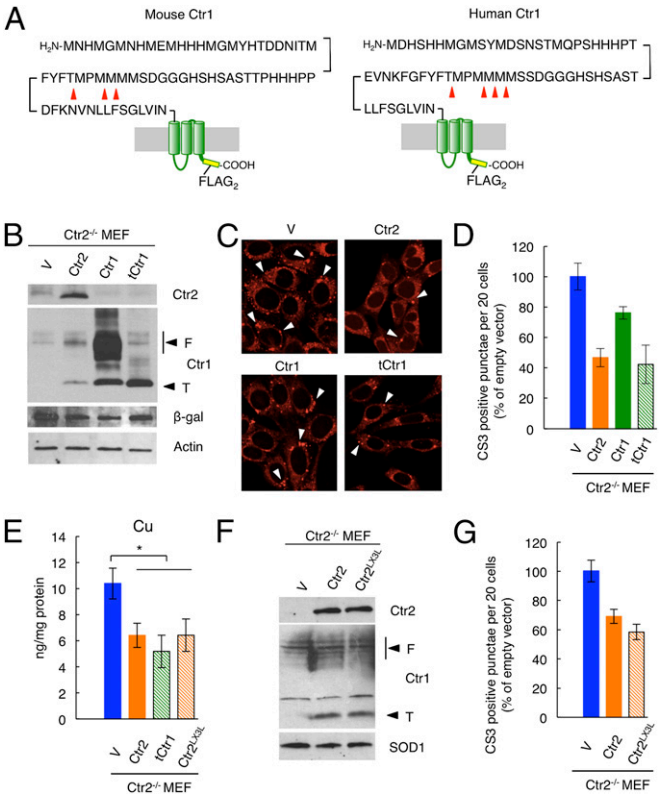

Fig. 6. Truncated Ctr1 mobilizes copper from endosomal compartments. (*A*) Red arrowheads indicate the cleavage sites determined for mouse and human Ctr1 (see Fig. S6 for band identification). (*B*) Ectopic expression of Ctr1 or truncated Ctr1 in $Ctr2^{-/-}$ MEFs. Protein extract was immunoblotted with anti-Ctr1, Ctr2, β-galactosidase antibody as transfection efficiency control, and anti-actin. (*C*) $Ctr2^{-/-}$ MEFs transfected in *B* were stained for Cu^{+} with CS3, and several fields (representative fields shown) were photographed for quantitation. (*D*) Enumeration of CS3-positive punctae for $Ctr2^{-/-}$ cells transfected with an empty vector (V), Ctr2, Ctr1, or truncated Ctr1 (tCtr1). (*E*) $Ctr2^{-/-}$ MEFs were analyzed for total Cu levels by ICP-MS. Expression of the Ctr2 cDNA (Ctr2), tCtr1, and $Ctr2^{LX3L}$, but not the empty expression vector (V) re-established low Cu levels. Data are presented as mean ± SD from three biological replicates. (*F*) A conserved Ctr1 motif is not required for Ctr2-induced cleavage of the Ctr1 ecto-domain. Protein extracts from $Ctr2^{-/-}$ MEFs transformed with vector (V) or a vector expressing Ctr2 or $Ctr2^{LX3L}$ were immunoblotted with anti-Ctr1, anti-Ctr2, or anti-SOD1 antibody. (*G*) Cells in *F* were stained and CS3-positive punctae were quantitated as in *D*.

Ctr1 reduced total cellular copper to similar levels as that achieved by returning Ctr2 to Ctr2$^{-/-}$ MEFs. These results suggest that truncated Ctr1 or changes in the ratio of truncated to full-length Ctr1 are important to mobilize copper out of the endosomal compartment, making it available for export out of the Ctr2$^{-/-}$ cells.

The data presented here support a model in which Ctr1 truncation is important for the mobilization of copper from endosomes. Given that Ctr2 shares topological similarity to Ctr1 and possesses an M-X$_3$-M motif in the second transmembrane domain that is essential for copper transport by Ctr1, it is possible that Ctr2 directly participates in the mobilization of endosomal copper stores, perhaps in a complex with truncated Ctr1. To test this hypothesis, we expressed wild-type Ctr2 in Ctr2$^{-/-}$ MEFs or a Ctr2 protein in which the M-X$_3$-M motif had been altered to L-X$_3$-L, which renders all known Ctr1 family Cu$^+$ transporters nonfunctional (16, 31). As shown in Fig. 6*F*, the Ctr2 protein in which the M-X$_3$-M motif has been altered to L-X$_3$-L is expressed at similar levels compared with wild-type Ctr2 and supports the accumulation of steady-state levels of truncated Ctr1 to an extent similar to wild-type Ctr2. Furthermore, expression of the Ctr2 L-X$_3$-L protein in Ctr2$^{-/-}$ MEFs resulted in the mobilization of copper from endosomal compartments and in reduction of total copper, similar to that stimulated by wild-type Ctr2 (Fig. 6 *E* and *G*). These results suggest that the conserved M-X$_3$-M motif is not necessary for Ctr2 to support the accumulation of truncated Ctr1 and for endosomal copper mobilization.

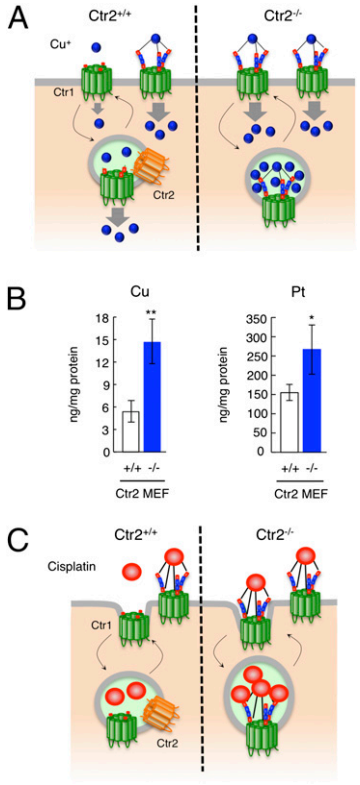

Fig. 7. Ctr2 modulates copper and cisplatin acquisition. (*A*) Model for Ctr1-dependent Cu$^+$ uptake and endosomal copper mobilization by truncated Ctr1. (*B*) Ctr2$^{-/-}$ MEFs accumulate cisplatin. Wild-type and Ctr2$^{-/-}$ MEFs were exposed to cisplatin and copper (*Left*) or platinum (Pt) (*Right*) measured by ICP-MS. Data are presented as mean ± SD for four biological replicates. (*C*) Model for Ctr1-dependent cisplatin import and the modulation of Pt uptake by truncation of Ctr1.

Ctr2 Modulates Copper and Cisplatin Accumulation. Ctr1 resides both on the plasma membrane and on endocytic vesicles, with constitutive internalization that is enhanced by its substrates, Cu$^+$ and cisplatin, and recycling (48, 49). The data presented here demonstrate that Ctr2 promotes the accumulation of truncated Ctr1 and suggest a model that truncated Ctr1 may be more active in mobilizing endosomal Cu stores (Fig. 7*A*). Cells expressing full-length Ctr1 were previously demonstrated to import Cu$^+$ and cisplatin more effectively than a version lacking the ecto-domain that harbors direct ligands for both copper and cisplatin (28). Moreover, previous studies suggested that depletion of Ctr2 by RNAi resulted in enhanced cisplatin accumulation via an unknown mechanism (50). Comparison of cisplatin accumulation in wild-type and Ctr2$^{-/-}$ MEFs demonstrated that Ctr2$^{-/-}$ cells accumulated approximately twice the levels of cisplatin over the course of the experiment, with elevated copper accumulation also observed (Fig. 7*B*). These results support the hypothesis that reduced cleavage of the Ctr1 ecto-domain in cells lacking Ctr2 facilitates cisplatin uptake by elevating the levels of full-length Ctr1 at the plasma membrane (Fig. 7*C*).

Discussion

Although the role of the Ctr1 family of Cu$^+$ importers in copper acquisition in organisms from yeast to mammals is well established, the mechanisms by which Ctr1 functions and is regulated are not well understood. Moreover, Ctr1 plays an important role in cellular uptake of cisplatin, and the levels of Ctr1 influence cisplatin accumulation in cellular and cancer models (25, 29, 35, 51). Here we present data that support a role for Ctr2 in regulating copper and cisplatin acquisition via Ctr1. Tissues, in particular brain tissue, from Ctr2$^{-/-}$ mice and Ctr2$^{-/-}$ MEFs accumulate copper in intracellular foci. We suggest that the copper deposits observed in mouse brain may also be in endosomal compartments, as observed in the Ctr2$^{-/-}$ MEFs. Interestingly, although tissues and MEFs from Ctr2$^{-/-}$ mice accumulate copper, results presented here suggest that the copper accumulated in Ctr2$^{-/-}$ cells or tissues is not bioavailable.

We previously demonstrated that mice with an intestinal epithelial cell (IEC)-specific excision of the *Ctr1* gene exhibit a peripheral copper deficiency, but accumulate copper in a nonlabile pool in IECs (22). We suggested that Ctr1 may function both in Cu$^+$ import from the apical membrane and in copper mobilization from an intracellular endosomal pool, perhaps generated and mobilized by endocytosis in a manner analogous to Fe transport by transferrin, the transferrin receptor, and the DMT1 divalent metal transporter (52). In the current work we similarly observe an intracellular copper pool from Ctr2$^{-/-}$ MEFs that we show cofractionates with the endosomal compartment. This same compartment is enriched for full-length and truncated Ctr1 and Ctr2 in wild-type MEFs, but for mostly full-length Ctr1 in Ctr2$^{-/-}$ MEFs. Based on the ability of truncated Ctr1 to more efficiently facilitate copper mobilization from the CS3-positive compartment compared with expression of full-length Ctr1 in Ctr2$^{-/-}$ MEFs, we suggest that truncated Ctr1 may be more active in copper mobilization from an endosomal compartment than full-length Ctr1. Moreover, previous studies in both yeast and mammalian cells suggest that Ctr1 harboring its copper-ligand–rich ecto-domain has a greater activity for extracellular Cu$^+$ import than truncated versions or mutants lacking the copper-coordinating methionine or histidine residues (31, 36, 47). Together, these observations and our current studies suggest a model in which full-length mammalian Ctr1 is the more active form for Cu$^+$ import across the plasma membrane, whereas cleavage of the Ctr1 ecto-domain generates a form that is more active for mobilizing endosomal copper stores (Fig. 7*A*). As Ctr1 is thought to function as a channel/permease for Cu$^+$ import, but as a receptor for cisplatin acquisition (27), this model is consistent with the accumulation of copper in endo-

somal compartments and cisplatin in an unknown subcellular location in cells or tissues lacking Ctr2.

Although a mechanism for the Ctr1 ecto-domain regulating copper export from an endosomal compartment has not yet been elucidated, structural studies suggest that the Ctr1 ecto-domain could occlude the Cu^+ pore formed at the homo-trimeric interface (42). Perhaps the structure of the Ctr1 ecto-domain or its interactions with other proteins is distinct when Ctr1 is localized to the cell surface, compared with the acidic endosomal compartment. Cleavage of this ecto-domain could provide a mechanism to alleviate this inhibitory function. The indirect involvement of Ctr2 in endosomal copper export is further supported by the observations that expression of Ctr2 in which the M-X_3-M motif has been altered to L-X_3-L fosters both accumulation of truncated Ctr1 and the mobilization of endosomal copper stores. Whereas the Ctr1 ecto-domain cleavage sites that we have determined by mass spectrometry are distinct from those predicted by others (46), the majority of Ctr1 truncations have retained one of two Met residues of the M-X-M sequence, both of which have been previously shown to be essential for Ctr1 Cu^+ transport activity (31).

Although Ctr2 was previously suggested to function as a direct lysosomal copper exporter (37), we suggest that Ctr2 participates in endosomal copper export by virtue of facilitating the cleavage of the Ctr1 ecto-domain or stabilizing truncated Ctr1, thereby driving Ctr1-dependent endosomal copper export. Consistent with a previous report suggesting that Ctr1 is cleaved in Rab9-positive endosomes (46), we find Ctr2 to be localized to the endosomal compartment, although it may also cycle to and from the plasma membrane or secretory compartment. Furthermore, because Ctr1 and Ctr2 interact in a complex, we speculate that Ctr2 enhances the abundance of truncated Ctr1 either by the recruitment of a protease or by stabilizing truncated Ctr1 against degradation. Current studies are underway to identify the protease activities responsible for Ctr1 cleavage and to understand how Ctr1 cleavage, or the stability of the cleaved form of Ctr1, is regulated by Ctr2 and potentially by copper status. Additional insights into these mechanisms may explain why Ctr2 influences the abundance of truncated Ctr1 in many, but not all, tissues. Finally, $Ctr2^{-/-}$ mice may be a useful tool for understanding how intracellular copper is stored and mobilized and how defects in this process may impact or be impacted by other disease states.

Materials and Methods

Animals. To generate Ctr2 knockout mice, loxP sequences were inserted between Ctr2 exons 1 and 2, and the PGKneo selection marker gene flanked by two loxP sites was inserted downstream of Ctr2 exon 4 (Ctr2-PGKneo-floxed). Mice having the Ctr2-PGKneo-floxed allele were crossbred with EIIa-Cre mice (Jackson Laboratory) to excise Ctr2 exons 2–4 and PGKneo. Mice were euthanized by CO_2 and perfused with PBS, and tissues were dissected, snap-frozen in liquid nitrogen, and stored at −80 °C until use. All procedures were approved by the Institutional Animal Care and Use Committee at Duke University.

PCR Genotyping, Blotting, and Quantitative RT-PCR. For DNA extraction, mouse tail tips or cells were lysed in lysis buffer consisting of 100 mM Tris·HCl (pH 7.4), 5 mM EDTA, 0.1% SDS, 200 mM NaCl, and 250 μg/mL Proteinase K in 1.5-mL centrifuge tubes at 50 °C for 3 h to overnight. The lysates were centrifuged at >12,000 × *g* for 10 min. DNA was extracted from the supernatants by standard methods. For RNA extraction, tissues perfused with PBS and dissected were immediately subjected to RNA extraction by the modified hot phenol method (53).

For Southern blotting, DNA extracted from clipped tail of 20- to 21-d-old mice was digested by EcoRV or EcoRI. Restriction enzyme sites and probes are indicated in Fig. S1*B*. For RNA blotting, membranes (Mouse NorthernLIGHT Blot, Panomics) were hybridized with cDNA probes for Ctr1 or Ctr2. Probes were generated by PCR and labeled with ^{32}P-dCTP with the Random Primers DNA Labeling System (Invitrogen). For semiquantitative RT-PCR, cDNA was synthesized by SuperScript III Kit (Invitrogen). SDS/PAGE and immunoblotting were carried out by standard protocols.

Cell Cultures. MEFs from $Ctr2^{+/+}$, $Ctr2^{+/-}$, and $Ctr2^{-/-}$ animals were generated as previously described (54). Wild-type ($Ctr1^{+/+}$) and $Ctr1^{-/-}$ MEFs were cultured in Dulbecco's Modified Eagle Medium (DMEM) (11995–065, Gibco) supplemented with 20% (vol/vol) heat-inactivated FBS, 1× MEM nonessential amino acids, 50 μg/mL uridine, 100 U/mL penicillin/streptomycin, and 55 μM 2-mercaptoethanol. Wild-type ($Ctr2^{+/+}$) and $Ctr2^{-/-}$ MEFs were cultured in DMEM supplemented with 10% (vol/vol) heat-inactivated FBS, 1× MEM nonessential amino acids, 2 mM Hepes, 1× antibiotic-antimycotic, 55 μM 2-mercaptoethanol, and 100 μg/mL hygromycin B. HEK293T cells were cultured in DMEM supplemented with 10% (vol/vol) heat-inactivated FBS and 100 U/mL penicillin/streptomycin. All cells were cultured under 5% CO_2 at 37 °C.

Protein Extraction. Tissue or cultured cell-protein extracts were prepared as follows. The tissues were homogenized in about 10 times volume of ice-cold lysis buffer [PBS (pH 7.4), 1% Triton X-100, 0.1% SDS, and 1 mM EDTA, proteinase inhibitors (complete EDTA-free, Roche; or Halt Proteinase Inhibitor Mixture, Thermo Scientific)]. Cell pellets were suspended in about 10 times volume of the same lysis buffer (ice-cold) and briefly vortexed. The tissue homogenates or cell suspensions were incubated in ice for 1 h and centrifuged at 16,000 × *g* at 4 °C for 20 min, and supernatants were collected. The protein concentrations were measured by DC Protein Assay Kit (Bio-Rad) or BCA Protein Assay Kit (Thermo Scientific).

Antibodies. A synthetic peptide of the sequence H2N-CLGPDQDSTGSRSTSDNRT-COOH, which corresponds to the cytosolic loop between transmembrane domains 1 and 2 of mouse Ctr2, was used to generate a rabbit anti-Ctr2 antiserum. Generation and affinity purification of the antiserum was performed by Bethyl Laboratories, Inc. The anti-Ctr1 antibody has been described previously (22). Antibodies against cytochrome *c* oxidase (CoxIV; MitoSciences), copper chaperone for Cu/Zn superoxide dismutase (CCS; FL-274; Santa Cruz Biotechnology), actin, glyceraldehyde 3-phosphate dehydrogenase (GAPDH) (Abcam), β-tubulin, Rab4, Rab5, Rab7, Rab9, Rab11, Lamp1 (Cell Signaling Technology), Cu/Zn superoxide dismutase (SOD1; Stressgen), c-Myc, FKBP15, and FLAG (M2; Sigma), β-galactosidase (Promega), ATP7A (generous gift from M. Petris, University of Missouri, Columbia, MO) were also used. Horseradish peroxidase-conjugated anti-mouse or anti-rabbit IgG (GE Healthcare Bio-Sciences) was used as the secondary antibody for immunoblotting. Alexa Fluor 488 or 568 anti-rabbit or anti-mouse IgG (Invitrogen) were used for immunofluorescence microscopy.

Metal Measurements by ICP-MS. Tissue, cell, or organelle Cu, Fe, and Zn concentrations were measured by ICP-MS as described (22). Tissues were collected into acid-washed 1.5-mL microcentrifuge tubes and weighed. The cultured cells were rinsed once with PBS, harvested by scraping in ice-cold PBS, and divided into two tubes. One tube was used to measure protein content, and the other sample was collected by centrifugation at 400 × *g* for 5 min at 4 °C. Tissues or cell pellets were suspended in 10 times volume/weight (μl/mg wet weight) of trace-analysis grade nitric acid (Sigma-Aldrich), heated at 85–95 °C for ∼1 h and subjected to ICP-MS analysis. For cisplatin accumulation, $Ctr2^{+/+}$ and $Ctr2^{-/-}$ cells were treated with 200 μM cisplatin (American Pharmaceutical Partners, Inc.) in Opti-MEM for 2 h and digested in HNO3:HCl (3:1) followed by ICP-MS. The analyses were performed by the Keck Elemental Geochemistry Laboratory, Department of Earth and Environmental Sciences, University of Michigan (Ann Arbor, MI) and by the Environmental and Agricultural Testing Service, Department of Soil Science, North Carolina State University (Raleigh, NC). Values were normalized by tissue wet weight or protein concentration.

XFM Analysis of Mouse Brains. For XFM experiments, saggittally oriented brain halves were embedded in optimal cryo temperature medium (OCT) Thermo Shandon) and flash-frozen in dry-ice–cooled iso-pentane and stored at −80 °C for sectioning. OCT blocks were sectioned at the Histopathology Shared Resource at Oregon Health and Science University using a cryostat (Mircom). For each sample, a 10-μm section was directly placed onto Ultralene (X-ray transparent film, 4 μm, Spex SamplePrep), air-dried, and stored in a desiccator until use. To be able to correlate regions of interest, adjacently cut 5-μm sections were stained with hematoxylin and eosin to image tissues. X-ray fluorescence microscopy data were collected on beamline 2-ID-E at the Advanced Photon Source, Argonne National Laboratory (Argonne, IL). Samples were mounted onto lucite sample holders [made in-house (55)] and fit into a kinematic sample mount. Target regions were selected using a light microscope (Leica) equipped with a motorized x, y-stage (Ludl Electronic Products). For the XFM measurements, the incident X-ray energy was tuned to 10 keV using a Si-monochromator with the monochromatic beam focused to ∼800 × 900 nm (final resolution) using a 20-cm Fresnel zone plate. The

sample was placed at 15° to the incident X-ray beam, and the resulting X-ray fluorescence was collected at 90° using an energy dispersive four-element detector (Vortex ME-4, SII Nanotechnology). X–y raster scans were performed in fly-scan mode (x-stage continuously moving) with a 30- × 30-μm pixel size and a 50-ms dwell time per pixel for coarse scans followed by several high-resolution scans with a 400- × 400-nm pixel size and an 8-ms dwell time per pixel for high-resolution scans. To optimize the fidelity of the image, X-ray fluorescence data were over-sampled in x and y. Elemental maps were created by extracting, background subtracting, and fitting the fluorescence counts for each element at each point using the program MAPS (56). For the analysis, to optimize the signal-to-background ratio and thus the visibility of elemental content, we calculated a running average spectrum for each pixel by averaging spectra of nine neighboring pixel and then carrying out the per-pixel fitting. The fluorescent photon counts were transformed into micrograms per square centimeter using calibrated X-ray standards (AXO products). Regions of interest were selected for each scan, and the respective elemental content was quantified.

Transfection. All plasmids used for the experiments except BiFC used the pcDNA3.1(+) backbone. For BiFC, the original plasmids pBiFC-bJun-YN155 and pBiFC-bFos-YC155 were provided by T. Kerppola (University of Michigan, Ann Arbor, MI). Transfection of plasmids into HEK293T cells was carried out by using Lipofectamine 2000 or Lipofectamine LTX (Invitrogen) according to the manufacturer's manual. Transfection into MEFs was carried out by electroporation using an Amaxa Nucleofection MEF2 kit or Amaxa SE Cell Line 4D-Nucleofector X Kit (Lonza).

Immunofluorescence Microscopy. HEK293T cells transfected with empty vector, $FLAG_2$, or c-Myc tagged Ctr1 or Ctr2 were fixed with 4% paraformaldehyde–PBS and permeabilized with 0.1% Triton X-100. For detection of extracellular epitopes, the Triton X-100 permeabilization step was omitted.

RNAi Knockdown. The smartpool siRNA for mouse *CTR1* (SLC31A1) or mouse *CTR2* (SLC31A2) (Dharmacon) was used to knock down the *CTR1 CTR2* genes, respectively, in the $Ctr2^{-/-}$ or $Ctr1^{-/-}$ MEFs. MEFs were seeded in six-well plates at a density of 1×10^6 cells/well. The following day siRNA or scrambled RNA (scRNA) (nontargeting RNA) was added to wells according to the manufacturer's instructions and incubated for 72 h before collection for ICP-MS and Western blot analysis.

Imaging Cu^+ Intracellular Copper in Live Cells by CS3 Probe. $Ctr2^{+/+}$ and $Ctr2^{-/-}$ MEFs were seeded in glass-bottom wells, incubated with 5 μM CS3 (gift from C. Chang, University of California, Berkeley, CA) in growth medium without serum for 15 min (57, 58). Live cells were observed by confocal microscopy (Leica DMI6000CS) using a diode laser at 561 nm. For transfected $Ctr2^{-/-}$ MEFs, coded counting of CS3-positive punctae was performed by three individuals for at least 100 cells over five fields of vision.

Discontinuous Density Gradient Fractionation of Cellular Compartments. The $Ctr2^{+/+}$ and $Ctr2^{-/-}$ MEFs were cultured on 15-cm diameter dishes until 100% confluent. The cells were rinsed twice with ice-cold PBS, scraped, and pelleted at 900 × *g* for 2 min at 4 °C. The 200-to 250-mg (wet weight) pellets were dissolved by slow vortexing in 800 μL lysis buffer with protease inhibitors, incubated in ice for 2 min, and subjected to sonication with 10 bursts in ice with a precooled probe. The lysates were centrifuged at 500 × *g* for 10 min 4 °C to precipitate the nuclei fraction. The supernatants were separated by discontinuous iodixanol density gradient centrifugation (Lysosomal Enrichment Kit, Thermo Scientific) at 145,000 × *g* for 2 h at 4 °C in a swing rotor. The three different fractions were collected from the gradient, and each fraction was divided into three tubes. One tube was subjected to a protein measurement by BCA Protein Assay Kit (Thermo Scientific), one tube was subjected to HNO_3 digestion for ICP-MS analysis, and one tube for protein isolation and immunoblotting.

Coimmunoprecipitation. HEK293T cells transfected with empty vector, c-Myc epitope-tagged Ctr2 (Myc-Ctr2), and FLAG epitope-tagged Ctr1 ($FLAG_2$-Ctr1), either alone or in combination and treated with or without the membrane-permeable cross-linker DSP. Ctr1 was immunoprecipitated with anti-FLAG antibody and extracts immunoblotted with anti-c-Myc antibody.

BiFC Assay. HEK293T cells were transfected with the pBiFC plasmids as described by Kerppola (43) as depicted in Fig. 4, incubated for 1–2 d, and observed with Zeiss Axio Imager wide-field fluorescence microscope (Zeiss).

Identification of Ctr1 Cleavage Sites. HEK293T cells transfected with control vector or human or mouse Ctr1 tagged with $FLAG_2$ at the carboxyl-terminus were cultured overnight, and FLAG-tagged proteins were affinity-purified with FLAG Affi-Gel, separated on SDS/PAGE gel, and stained with a Colloidal Blue Staining Kit (Invitrogen). The band corresponding to the truncated form of Ctr1 was excised, digested in-gel by trypsin, and subjected to peptide analysis and sequencing by LC-MS/MS performed by the Duke University Proteomics Core.

ACKNOWLEDGMENTS. We thank members of the D.J.T. laboratory for suggestions; C. Jones and K. McNaughton Raney for expert technical assistance; the Duke University Proteomics Core Facility; T. Kerppola for BiFC reagents; S. Dodani and C. Chang for CS-3; S. Vogt at the Advanced Photon Source for data analysis and beamline support; M. Duffy from the Oregon Health and Science University (OHSU) Elemental Analysis Core; and K. Forquer from the Histopathology Shared Resource at the Oregon Knight Cancer Institute. This work was supported by National Institutes of Health (NIH) Grants DK074192 (to D.J.T.) and GM090016 (to M.R.) and by Postdoctoral Fellowship K2012-77PK-21938-01-2 from the Swedish Research Council and The Thorne-Holst Foundation (to H.Ö.). The Advanced Photon Source was supported by the Department of Energy, Office of Science Contract DE-AC-0206CH11357.

1. Kim BE, Nevitt T, Thiele DJ (2008) Mechanisms for copper acquisition, distribution and regulation. *Nat Chem Biol* 4(3):176–185.
2. Wang Y, Hodgkinson V, Zhu S, Weisman GA, Petris MJ (2011) Advances in the understanding of mammalian copper transporters. *Adv Nutr* 2(2):129–137.
3. Collins JF, Prohaska JR, Knutson MD (2010) Metabolic crossroads of iron and copper. *Nutr Rev* 68(3):133–147.
4. Barnham KJ, Bush AI (2008) Metals in Alzheimer's and Parkinson's diseases. *Curr Opin Chem Biol* 12(2):222–228.
5. Kaler SG (2011) ATP7A-related copper transport diseases-emerging concepts and future trends. *Nat Rev Neurol* 7(1):15–29.
6. Lutsenko S, Barnes NL, Bartee MY, Dmitriev OY (2007) Function and regulation of human copper-transporting ATPases. *Physiol Rev* 87(3):1011–1046.
7. Prohaska JR, Lukasewycz OA (1990) Effects of copper deficiency on the immune system. *Adv Exp Med Biol* 262:123–143.
8. Madsen E, Gitlin JD (2007) Copper and iron disorders of the brain. *Annu Rev Neurosci* 30:317–337.
9. Medeiros DM, Davidson J, Jenkins JE (1993) A unified perspective on copper deficiency and cardiomyopathy. *Proc Soc Exp Biol Med* 203(3):262–273.
10. Dancis A, Haile D, Yuan DS, Klausner RD (1994) The Saccharomyces cerevisiae copper transport protein (Ctr1p). Biochemical characterization, regulation by copper, and physiologic role in copper uptake. *J Biol Chem* 269(41): 25660–25667.
11. Pena MM, Puig S, Thiele DJ (2000) Characterization of the Saccharomyces cerevisiae high affinity copper transporter Ctr3. *J Biol Chem* 275(43):33244–33251.
12. Sancenón V, Puig S, Mira H, Thiele DJ, Peñarrubia L (2003) Identification of a copper transporter family in Arabidopsis thaliana. *Plant Mol Biol* 51(4):577–587.
13. Turski ML, Thiele DJ (2007) Drosophila Ctr1A functions as a copper transporter essential for development. *J Biol Chem* 282(33):24017–24026.
14. Riggio M, et al. (2002) High affinity copper transport protein in the lizard Podarcis sicula: Molecular cloning, functional characterization and expression in somatic tissues, follicular oocytes and eggs. *Biochim Biophys Acta* 1576(1–2):127–135.
15. Lee J, Prohaska JR, Dagenais SL, Glover TW, Thiele DJ (2000) Isolation of a murine copper transporter gene, tissue specific expression and functional complementation of a yeast copper transport mutant. *Gene* 254(1–2):87–96.
16. Pope CR, Flores AG, Kaplan JH, Unger VM (2012) Structure and function of copper uptake transporters. *Curr Top Membr* 69:97–112.
17. Nose Y, et al. (2010) Ctr1 is an apical copper transporter in mammalian intestinal epithelial cells in vivo that is controlled at the level of protein stability. *J Biol Chem* 285(42):32385–32392.
18. Klomp AE, Tops BB, Van Denberg IE, Berger R, Klomp LW (2002) Biochemical characterization and subcellular localization of human copper transporter 1 (hCTR1). *Biochem J* 364(Pt 2):497–505.
19. Kuo YM, Gybina AA, Pyatskowit JW, Gitschier J, Prohaska JR (2006) Copper transport protein (Ctr1) levels in mice are tissue specific and dependent on copper status. *J Nutr* 136(1):21–26.
20. Kim H, Son HY, Bailey SM, Lee J (2009) Deletion of hepatic Ctr1 reveals its function in copper acquisition and compensatory mechanisms for copper homeostasis. *Am J Physiol Gastrointest Liver Physiol* 296(2):G356–G364.
21. Lee J, Prohaska JR, Thiele DJ (2001) Essential role for mammalian copper transporter Ctr1 in copper homeostasis and embryonic development. *Proc Natl Acad Sci USA* 98(12):6842–6847.
22. Nose Y, Kim BE, Thiele DJ (2006) Ctr1 drives intestinal copper absorption and is essential for growth, iron metabolism, and neonatal cardiac function. *Cell Metab* 4(3): 235–244.
23. Kim BE, et al. (2010) Cardiac copper deficiency activates a systemic signaling mechanism that communicates with the copper acquisition and storage organs. *Cell Metab* 11(5):353–363.

24. Kuo YM, Zhou B, Cosco D, Gitschier J (2001) The copper transporter CTR1 provides an essential function in mammalian embryonic development. *Proc Natl Acad Sci USA* 98(12):6836–6841.
25. Ishida S, Lee J, Thiele DJ, Herskowitz I (2002) Uptake of the anticancer drug cisplatin mediated by the copper transporter Ctr1 in yeast and mammals. *Proc Natl Acad Sci USA* 99(22):14298–14302.
26. Kuo MT, Fu S, Savaraj N, Chen HH (2012) Role of the human high-affinity copper transporter in copper homeostasis regulation and cisplatin sensitivity in cancer chemotherapy. *Cancer Res* 72(18):4616–4621.
27. Sinani D, Adle DJ, Kim H, Lee J (2007) Distinct mechanisms for Ctr1-mediated copper and cisplatin transport. *J Biol Chem* 282(37):26775–26785.
28. Larson CA, et al. (2010) The role of the N-terminus of mammalian copper transporter 1 in the cellular accumulation of cisplatin. *Biochem Pharmacol* 80(4):448–454.
29. Howell SB, Safaei R, Larson CA, Sailor MJ (2010) Copper transporters and the cellular pharmacology of the platinum-containing cancer drugs. *Mol Pharmacol* 77(6): 887–894.
30. Chen HH, et al. (2012) Predictive and prognostic value of human copper transporter 1 (hCtr1) in patients with stage III non-small-cell lung cancer receiving first-line platinum-based doublet chemotherapy. *Lung Cancer* 75(2):228–234.
31. Puig S, Lee J, Lau M, Thiele DJ (2002) Biochemical and genetic analyses of yeast and human high affinity copper transporters suggest a conserved mechanism for copper uptake. *J Biol Chem* 277(29):26021–26030.
32. Crider SE, Holbrook RJ, Franz KJ (2010) Coordination of platinum therapeutic agents to met-rich motifs of human copper transport protein1. *Metallomics* 2(1):74–83.
33. Jiang J, Nadas IA, Kim MA, Franz KJ (2005) A Mets motif peptide found in copper transport proteins selectively binds Cu(I) with methionine-only coordination. *Inorg Chem* 44(26):9787–9794.
34. Du X, et al. (2013) Kinetics and thermodynamics of metal binding to the N-terminus of a human copper transporter, hCTR1. *Chem Commun (Camb)* 49(80):9134–9136.
35. Larson CA, Adams PL, Blair BG, Safaei R, Howell SB (2010) The role of the methionines and histidines in the transmembrane domain of mammalian copper transporter 1 in the cellular accumulation of cisplatin. *Mol Pharmacol* 78(3):333–339.
36. Maryon EB, Molloy SA, Kaplan JH (2007) O-linked glycosylation at threonine 27 protects the copper transporter hCTR1 from proteolytic cleavage in mammalian cells. *J Biol Chem* 282(28):20376–20387.
37. van den Berghe PV, et al. (2007) Human copper transporter 2 is localized in late endosomes and lysosomes and facilitates cellular copper uptake. *Biochem J* 407(1): 49–59.
38. Blair BG, et al. (2011) Copper transporter 2 regulates endocytosis and controls tumor growth and sensitivity to cisplatin in vivo. *Mol Pharmacol* 79(1):157–166.
39. Bertinato J, Swist E, Plouffe LJ, Brooks SP, L'abbé MR (2008) Ctr2 is partially localized to the plasma membrane and stimulates copper uptake in COS-7 cells. *Biochem J* 409(3):731–740.
40. Molloy SA, Kaplan JH (2009) Copper-dependent recycling of hCTR1, the human high affinity copper transporter. *J Biol Chem* 284(43):29704–29713.
41. Vogt S, Ralle M (2013) Opportunities in multidimensional trace metal imaging: Taking copper-associated disease research to the next level. *Anal Bioanal Chem* 405(6): 1809–1820.
42. De Feo CJ, Aller SG, Siluvai GS, Blackburn NJ, Unger VM (2009) Three-dimensional structure of the human copper transporter hCTR1. *Proc Natl Acad Sci USA* 106(11): 4237–4242.
43. Kerppola TK (2006) Design and implementation of bimolecular fluorescence complementation (BiFC) assays for the visualization of protein interactions in living cells. *Nat Protoc* 1(3):1278–1286.
44. Gybina AA, Prohaska JR (2006) Variable response of selected cuproproteins in rat choroid plexus and cerebellum following perinatal copper deficiency. *Genes Nutr* 1(1):51–59.
45. Caruano-Yzermans AL, Bartnikas TB, Gitlin JD (2006) Mechanisms of the copper-dependent turnover of the copper chaperone for superoxide dismutase. *J Biol Chem* 281(19):13581–13587.
46. Maryon EB, Zhang J, Jellison JW, Kaplan JH (2009) Human copper transporter 1 lacking O-linked glycosylation is proteolytically cleaved in a Rab9-positive endosomal compartment. *J Biol Chem* 284(41):28104–28114.
47. Haas KL, Putterman AB, White DR, Thiele DJ, Franz KJ (2011) Model peptides provide new insights into the role of histidine residues as potential ligands in human cellular copper acquisition via Ctr1. *J Am Chem Soc* 133(12):4427–4437.
48. Petris MJ, Smith K, Lee J, Thiele DJ (2003) Copper-stimulated endocytosis and degradation of the human copper transporter, hCtr1. *J Biol Chem* 278(11):9639–9646.
49. Holzer AK, Howell SB (2006) The internalization and degradation of human copper transporter 1 following cisplatin exposure. *Cancer Res* 66(22):10944–10952.
50. Blair BG, Larson CA, Safaei R, Howell SB (2009) Copper transporter 2 regulates the cellular accumulation and cytotoxicity of Cisplatin and Carboplatin. *Clin Cancer Res* 15(13):4312–4321.
51. Guo Y, Smith K, Petris MJ (2004) Cisplatin stabilizes a multimeric complex of the human Ctr1 copper transporter: Requirement for the extracellular methionine-rich clusters. *J Biol Chem* 279(45):46393–46399.
52. Zhao N, Enns CA (2012) Iron transport machinery of human cells: Players and their interactions. *Curr Top Membr* 69:67–93.
53. Schmitt ME, Brown TA, Trumpower BL (1990) A rapid and simple method for preparation of RNA from Saccharomyces cerevisiae. *Nucleic Acids Res* 18(10): 3091–3092.
54. Lee J, Petris MJ, Thiele DJ (2002) Characterization of mouse embryonic cells deficient in the ctr1 high affinity copper transporter. Identification of a Ctr1-independent copper transport system. *J Biol Chem* 277(43):40253–40259.
55. Ralle M, Lutsenko S (2009) Quantitative imaging of metals in tissues. *Biometals* 22(1): 197–205.
56. Vogt S (2003) Maps: A set of software tools for analysis and visualization of 3D X-ray fluorescent datasets. *J Phys IV* 104:635–638.
57. Dodani SC, et al. (2011) Calcium-dependent copper redistributions in neuronal cells revealed by a fluorescent copper sensor and X-ray fluorescence microscopy. *Proc Natl Acad Sci USA* 108(15):5980–5985.
58. Zeng L, Miller EW, Pralle A, Isacoff EY, Chang CJ (2006) A selective turn-on fluorescent sensor for imaging copper in living cells. *J Am Chem Soc* 128(1):10–11.